

Prior Knowledge-enhanced Spatio-temporal Epidemic Forecasting

Sijie Ruan¹, Jinyu Li¹, Jia Wei¹, Zenghao Xu², Jie Bao³, Junshi Xu⁴,
Junyang Qiu⁵, Hanning Yuan¹, Xiaoxiao Wang², Shuliang Wang¹

¹Beijing Institute of Technology, China ²Zhejiang Center for Disease Control and Prevention, China

³JD Technology, China ⁴The University of Hong Kong, Hong Kong SAR, China

⁵China Mobile Internet, China

{sjruan, lly666, 1120230622, yhn6, slwang2011}@bit.edu.cn, {zhxu, xxwang}@cdc.zj.cn,
baojie@jd.com, junshixu@hku.hk, qiujunyang@139.com

Abstract

Spatio-temporal epidemic forecasting is critical for public health management, yet existing methods often struggle with insensitivity to weak epidemic signals, over-simplified spatial relations, and unstable parameter estimation. To address these challenges, we propose the Spatio-Temporal priO-raware Epidemic Predictor (STOEP), a novel hybrid framework that integrates implicit spatio-temporal priors and explicit expert priors. STOEP consists of three key components: (1) Case-aware Adjacency Learning (CAL), which dynamically adjusts mobility-based regional dependencies using historical infection patterns; (2) Space-informed Parameter Estimating (SPE), which employs learnable spatial priors to amplify weak epidemic signals; and (3) Filter-based Mechanistic Forecasting (FMF), which uses an expert-guided adaptive thresholding strategy to regularize epidemic parameters. Extensive experiments on real-world COVID-19 and influenza datasets demonstrate that STOEP outperforms the best baseline by 11.1% in RMSE. The system has been deployed at one provincial CDC in China to facilitate downstream applications.

1 Introduction

Population-level epidemic forecasting is of great importance to public health management, since accurate forecasting of new infections at each location can help governments and healthcare providers allocate resources, design intervention policies, and evaluate the effectiveness of control measures [Qian *et al.*, 2021].

In the early years, constrained by data scarcity, epidemic forecasting primarily relied on mechanistic models, e.g., SIR [Kermack and McKendrick, 1927]. With the rise of deep learning, data-driven approaches have been increasingly adopted in this field [Arora *et al.*, 2020]. Simultaneously, realizing the spatial dependencies of disease transmission among regions, spatio-temporal forecasting across multiple regions jointly has garnered great attention [Deng *et al.*, 2020].

However, due to the limited epidemiological data, these models remain prone to overfitting. In recent years, there

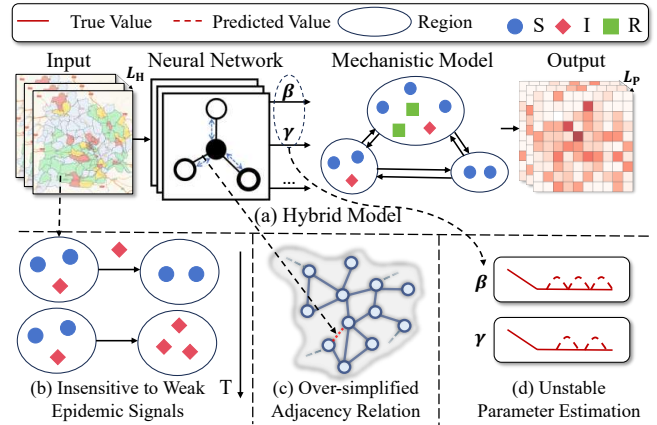


Figure 1: (a) Illustrations of hybrid models; (b) Insensitivity to weak epidemic signals.; (c) Over-simplified adjacency relation; (d) Unstable parameter estimation.

has been a surge focused on hybrid models that integrate mechanistic principles with deep learning [Cao *et al.*, 2022; Wang *et al.*, 2022; Han *et al.*, 2025], e.g., employing deep neural networks to estimate the parameters of mechanistic models as shown in Figure 1(a). Nevertheless, existing methods still encounter three primary limitations:

- **Insensitivity to Weak Epidemic Signals.** Unlike traffic forecasting, epidemic data often contain weak signals as shown in Figure 1(b). That is, the confirmed cases in most of time are small, but infectious diseases can surge to high prevalence levels in a short time. Existing deep-learning modules [Wu *et al.*, 2019] are often insensitive to such weak yet critical signals, leading to missed early warnings.
- **Over-simplified Adjacency Relation.** Existing methods capture the spatial dependency by using the human mobility intensities among regions [Wang *et al.*, 2018; Cao *et al.*, 2022]. Though the vital factor, i.e., human mobility for disease transmission, is considered, they omit the intrinsic similarities among regions as shown in Figure 1(c).
- **Unstable Parameter Estimation.** As mentioned, hybrid models rely on neural networks to produce vital epidemic parameters. However, unconstrained network outputs often fluctuate violently in data-scarce scenarios as shown in

Figure 1(d), resulting in mechanically implausible and unstable parameter estimation.

An intuitive idea to tackle those issues is to incorporate the external epidemic knowledge to regulate the modeling process. However, related data may not always be available. To this end, in this paper, we propose **S**patio-**T**emporal **p**riOr-aware **E**pidemic **P**redictor (STOEP), which incorporates two types of implicit knowledge without the requirements of external data, i.e., spatio-temporal priors and expert priors, to facilitate the epidemic modeling. The spatio-temporal priors are derived from data to enhance the representation of each region even if the signals are weak, and adjust the adjacency relation among regions in addition to the mobility data, while the expert priors are obtained from domain experts to regularize the output of estimated epidemic parameters to stabilize the epidemic forecasting. More specifically, STOEP is composed of three modules: (1) *Case-aware Adjacency Learning (CAL)*, which dynamically fuses mobility data with patterns of confirmed cases by a learnable pattern memory to capture temporal epidemic priors dynamically; (2) *Space-informed Parameter Estimating (SPE)*, which introduces a specialized spatial enhancement block with learnable spatial priors to explicitly amplify signals; (3) *Filter-based Mechanistic Forecasting (FMF)*, which employs an adaptive thresholding strategy guided by expert priors to suppress noise in data-scarce regions. The main contributions are summarized as follows:

- We inject spatio-temporal priors into the epidemic forecasting model, which makes adjacency relation aware of temporal patterns via CAL, and makes model inputs enhanced by spatial knowledge via SPE.
- We propose an expert prior-guided adaptive thresholding strategy via FMF to stabilize the epidemic forecasting by regularizing the output of estimated epidemic parameters.
- Extensive experiments on two real-world epidemic datasets, i.e., COVID-19 and influenza, demonstrate that STOEP outperforms the best baseline by 11.1% on average in RMSE. We also released the code for public use¹.
- A system based on STOEP is deployed and used in one provincial CDC in China to facilitate downstream applications.

2 Preliminaries

2.1 Definitions

Definition 1 (Daily Confirmed Cases). We denote the number of daily confirmed cases in region n at day τ as x_n^τ , and the number of daily confirmed cases over all regions as $\mathbf{X}^\tau \in \mathbb{R}^N$, where N is the number of regions.

Definition 2 (Historical Observations). To make the epidemic forecasting model work effectively, we divide historical observations into two types, i.e., essential factors and optional factors. The essential factors include historical daily confirmed cases $\mathbf{X}^{t-(T_{in}-1):t}$, susceptible population

$\mathbf{S}^{t-(T_{in}-1):t} \in \mathbb{R}^{N \times T_{in}}$, infected population $\mathbf{I}^{t-(T_{in}-1):t} \in \mathbb{R}^{N \times T_{in}}$ and recovered population $\mathbf{R}^{t-(T_{in}-1):t} \in \mathbb{R}^{N \times T_{in}}$, where T_{in} is the given lookback time window. Other related features can also be incorporated as optional factors, e.g., day of week. We denote historical observations as $\mathcal{O}^{t-(T_{in}-1):t} \in \mathbb{R}^{N \times T_{in} \times C}$, where $C \geq 4$ is the number of factors considered.

Definition 3 (Historical Mobility Data). We use historical mobility data $\mathcal{M}^{t-(T_{in}-1):t} \in \mathbb{R}^{N \times N \times T_{in}}$ to characterize the mobility intensity among different regions, where entry $m_{ij}^\tau \geq 0$ denotes the flow intensity from region i to region j at time $\tau \in \{t - (T_{in} - 1), \dots, t\}$.

2.2 Problem Statement

Given the historical observations $\mathcal{O}^{t-(T_{in}-1):t} \in \mathbb{R}^{N \times T_{in} \times C}$ and mobility data $\mathcal{M}^{t-(T_{in}-1):t} \in \mathbb{R}^{N \times N \times T_{in}}$, predict the daily confirmed cases in the future T_{out} timesteps, i.e., $\hat{\mathbf{X}}^{t+1:t+T_{out}} \in \mathbb{R}^{N \times T_{out}}$, which can be formulated as:

$$\{\mathcal{O}^{t-(T_{in}-1):t}, \mathcal{M}^{t-(T_{in}-1):t}\} \xrightarrow{f(\cdot)} \hat{\mathbf{X}}^{t+1:t+T_{out}} \quad (1)$$

3 Methodology

STOEP follows the paradigm of hybrid spatio-temporal epidemic forecasting, which essentially leverages a mechanistic model to forecast future confirmed cases, but the epidemic parameters of the model are estimated by neural networks. The architecture of STOEP is depicted in Figure 2, which consists of three modules:

- **Case-aware Adjacency Learning (CAL)**, which takes historical mobility data as well as daily confirmed cases, and produces a case-aware adjacency matrix. It would be used to indicate the adjacency intensities.
- **Space-informed Parameter Estimating (SPE)**, which takes historical observations, learned spatial priors and case-aware adjacency matrix, to estimate the epidemic parameters of the mechanistic model.
- **Filter-based Mechanistic Forecasting (FMF)**, which takes estimated epidemic parameters as well as the human mobility data, predicts the future daily confirmed cases via a filter-based mechanistic model.

The complexity and scalability of STOEP is practical for real-world use, and the detailed analysis is given in Appendix A. Next, we elaborate on each module in detail.

3.1 Case-aware Adjacency Learning

Case-aware adjacency learning (CAL) aims to learn the case-aware adjacency intensities among different regions $\mathbf{A} \in \mathbb{R}^{N \times N}$ based on the historical mobility data $\mathcal{M}^{t-(T_{in}-1):t}$ and daily confirmed cases $\mathbf{X}^{t-(T_{in}-1):t}$.

Main Idea. As mentioned, to adequately model the adjacency relation among regions, we fuse the mobility-based intensities with data-derived intensities. The main idea is to

¹<https://github.com/Tracker1701/STOEP-Epidemic-Forecasting>

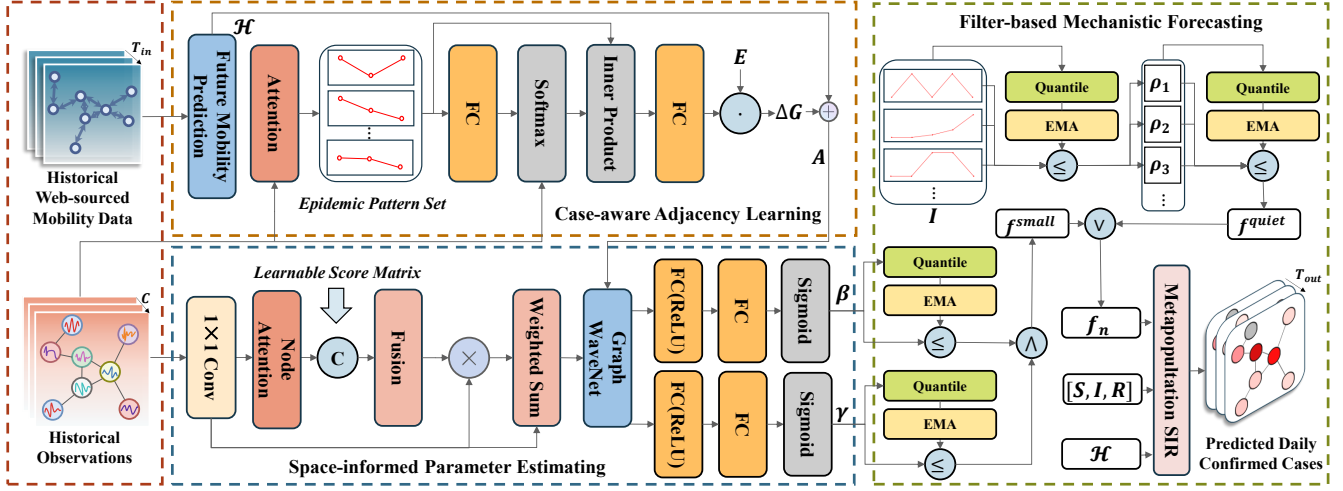


Figure 2: Framework of proposed epidemic forecasting model STOEP.

adjust the mobility-based intensities using data-derived adjacency relationship, which are detailed as follows.

Mobility-based Adjacency Learning. We first perform a linear transformation from past to future on \mathcal{M} to obtain the future mobility prediction $\mathcal{H}^{t+1:t+T_{\text{out}}} \in \mathbb{R}^{N \times N \times T_{\text{out}}}$. And the mobility-based adjacency matrix $\mathbf{A}_m \in \mathbb{R}^{N \times N}$ can be derived by mean-pooling over the prediction horizons:

$$\mathbf{A}_m = \frac{1}{T_{\text{out}}} \sum_{i=1}^{T_{\text{out}}} \mathcal{H}^{t+i} \quad (2)$$

Case-aware Adjacency Adjustment. For each region, its recent observation of confirmed cases may contain some noise. To quantify its correlation with other regions based on the recently observed cases, we first perform a soft clustering to obtain its robust representation, and then use the representation to calculate the intensity with other regions.

More specifically, for a historical daily confirmed case of region n , i.e., $\mathbf{x}_n^{t-(T_{\text{in}}-1):t}$, we take its most recent S days ($S \leq T_{\text{in}}$) to form a recent observation $\mathbf{x}_n^{t-(S-1):t}$. $\mathbf{x}_n^{t-(S-1):t}$ would be normalized to eliminate the effect of population disparity to form an epidemic pattern $\tilde{\mathbf{x}}_n^{t-(S-1):t}$. Then the robust representation $\mathbf{r}_n \in \mathbb{R}^{d_A}$ of the current epidemic pattern of region n can be derived by attention-based pattern retrieval from a learnable pattern set $\mathbf{P} \in \mathbb{R}^{P \times S}$:

$$\alpha_n = \text{softmax}\left(\frac{\mathbf{q}_n \mathbf{K}^\top}{\sqrt{d}}\right), \quad \mathbf{r}_n = \text{FC}(\alpha_n \mathbf{V}) \quad (3)$$

where α_n are the attention weights of region n over P patterns, $\mathbf{K} \in \mathbb{R}^d$ and $\mathbf{V} \in \mathbb{R}^d$ are transformed key and value matrix of \mathbf{P} . After that, \mathbf{r}_n would be compared with vectors in a learnable region embedding table $\mathbf{E} \in \mathbb{R}^{N \times d_A}$ to obtain its recent correlation with other regions. Formally, the case-based adjacency intensity ΔG_{nm} of region n to region m is:

$$\Delta G_{nm} = \alpha \cdot \langle \mathbf{r}_n, \mathbf{e}_m \rangle \quad (4)$$

where $\mathbf{e}_m \in \mathbb{R}^{d_A}$ is entry m of \mathbf{E} , $\langle \cdot, \cdot \rangle$ denotes the inner product. α is a learnable scalar that scales the correction strength, which is initialized as 0 to prevent training perturbations. Finally, the case-based adjacency $\Delta \mathbf{G} \in \mathbb{R}^{N \times N}$ serves as a residual term to adjust the mobility-based adjacency \mathbf{A}_m to obtain the final adjacency matrix \mathbf{A} :

$$\mathbf{A} = \mathbf{A}_m + \Delta \mathbf{G} \quad (5)$$

3.2 Space-informed Parameter Estimating

Space-informed parameter estimating (SPE) aims to learn epidemic parameters of the mechanistic model. In this work, we leverage MetaSIR [Wang *et al.*, 2018] as the mechanistic model, since it can jointly model multiple regions. The basic principle of MetaSIR can be found in Appendix F. In the context of MetaSIR, STOEP needs to estimate the infection rate $\beta \in \mathbb{R}^{N \times T_{\text{out}}}$ and recovery rate $\gamma \in \mathbb{R}^{N \times T_{\text{out}}}$ of different regions in future time steps.

Main Idea. To amplify the weak signals in epidemic data, we aim to explicitly learn some stable spatial dependency, which would be fused with dynamic dependency derived from historical observations, to comprehensively enhance the input features. After that, the enhanced features are fed into GraphWaveNet [Wu *et al.*, 2019] to estimate β and γ , which are detailed as follows.

Dynamic Dependency Generation. We first transform the historical observations $\mathcal{O}^{t-(T_{\text{in}}-1):t}$ to a hidden representation $\mathbf{X}_c \in \mathbb{R}^{N \times T_{\text{in}} \times C_c}$ by a 1×1 convolution. We compute the inter-region dynamic dependency attention map $\mathbf{A}^{\text{node}} \in \mathbb{R}^{N \times N}$ by applying multi-head self-attention to \mathbf{X}_c for every input step, and averaging the scores over time and heads:

$$\mathbf{A}^{\text{node}} = \frac{1}{HT_{\text{in}}} \sum_{h,t} \text{Attn}_h(\mathbf{X}_{c,t}^{(h)}). \quad (6)$$

where H is the number of heads.

Spatial Prior Incorporation. To capture stable and long-range spatial dependency, we introduce a learnable score ma-

trix $\mathbf{S} \in \mathbb{R}^{N \times N}$ that encodes a global spatial prior. \mathbf{S} is initialized as an identity matrix and optimized during the training. We apply a row-wise softmax on \mathbf{S} to obtain a static dependency attention map $\mathbf{A}^{\text{struct}} = \text{softmax}_{\text{row}}(\mathbf{S})$.

We use a gating mechanism to fuse the dynamic dependency and the static dependency to obtain a fused attention map $\mathbf{A}^{\text{fuse}} \in \mathbb{R}^{N \times N}$ as follows:

$$\begin{aligned} \Gamma &= \phi([\mathbf{A}^{\text{node}}; \mathbf{A}^{\text{struct}}]) \\ \mathbf{A}^{\text{fuse}} &= \sigma(\Gamma) \odot \mathbf{A}^{\text{node}} + (1 - \sigma(\Gamma)) \odot \mathbf{A}^{\text{struct}} \end{aligned} \quad (7)$$

where $[\cdot; \cdot]$ is the concatenation, $\phi(\cdot)$ is a linear layer to produce a gate $\Gamma \in \mathbb{R}^{N \times N}$, $\sigma(\cdot)$ is sigmoid activation, and \odot is Hadamard product. After that, we regularize \mathbf{A}^{fuse} by symmetrizing, enforcing nonnegativity, and row-normalizing to obtain an refined attention map $\mathbf{A}_{\text{norm}}^{\text{fuse}} \in \mathbb{R}^{N \times N}$.

Feature Enhancement. Based on $\mathbf{A}_{\text{norm}}^{\text{fuse}}$, we enhance the features \mathbf{X}_c in a residual connection manner:

$$\begin{aligned} \bar{\mathbf{X}}_c &= \mathbf{A}_{\text{norm}}^{\text{fuse}} \mathbf{X}_c \\ \tilde{\mathbf{O}}^{t-(T_{\text{in}}-1):t} &= (1 - \epsilon) \mathbf{X}_c + \epsilon \bar{\mathbf{X}}_c \end{aligned} \quad (8)$$

where $\tilde{\mathbf{O}}^{t-(T_{\text{in}}-1):t} \in \mathbb{R}^{N \times T_{\text{in}} \times C_c}$ is the feature enhanced input, and $\epsilon \in [0, 1]$ is a learnable scalar (initialized as 0).

Parameter Estimation. After node features are enhanced, we feed $\tilde{\mathbf{O}}^{t-(T_{\text{in}}-1):t}$ as well as the adjacency matrix \mathbf{A} obtained in CAL into GraphWaveNet-style backbone [Wu *et al.*, 2019] for spatio-temporal modeling to obtain the hidden representation $\mathbf{Z} \in \mathbb{R}^{N \times T_{\text{out}} \times d}$:

$$\mathbf{Z} = \text{GraphWaveNet}(\tilde{\mathbf{O}}^{t-(T_{\text{in}}-1):t}, \mathbf{A}) \quad (9)$$

Finally, two linear heads take the hidden representation and predict the epidemiological parameters $\beta \in \mathbb{R}^{N \times T_{\text{out}}}$ and $\gamma \in \mathbb{R}^{N \times T_{\text{out}}}$ for each node on future time steps:

$$\beta = \sigma(\text{FC}_{\beta}(\mathbf{Z})), \quad \gamma = \sigma(\text{FC}_{\gamma}(\mathbf{Z})) \quad (10)$$

3.3 Filter-based Mechanistic Forecasting

Filter-based mechanistic forecasting (FMF) aims to forecast future daily confirmed cases $\hat{\mathbf{X}}^{t+1:t+T_{\text{out}}}$ based on the estimated epidemic parameters β and γ from SPE via a filter-based MetaSIR.

Main Idea. To mitigate the instability of epidemic parameter estimation, by discussing with the domain experts, we suppress the disease transmission process if estimated epidemic parameters or infected population are small. A straightforward idea is to set a constant threshold to suppress the epidemic parameters. However, due to the heterogeneity across space and time, we propose an adaptive thresholding strategy to flexibly decide whether the disease transmission process should be suppressed or not, which are detailed as follows.

Adaptive Thresholding Strategy. Adaptive thresholding strategy aims to learn an adaptive threshold given a set of numbers, e.g., $\{v_r\}_{r=1}^R$. We first compute the quantile $\kappa = \text{Quantile}(\{v_r\}_{r=1}^R, \kappa)$, where κ is the desired quantile ratio. During the training, κ would be smoothed by Exponential Moving Average (EMA) to control the adaptivity–stability trade-off. The adaptive threshold is defined as

$$\delta = \max\{\kappa, \delta_{\min}\}, \quad (11)$$

where δ_{\min} is a safeguard lower bound to avoid vanishing thresholds when the quantile becomes very small.

Small Parameter Detection. Small parameter detection aims to detect whether the estimated epidemic parameters $\beta_n \in \mathbb{R}^{T_{\text{out}}}$ and $\gamma_n \in \mathbb{R}^{T_{\text{out}}}$ of a region n are sufficiently small. For each region n , we first obtain its maximum parameter estimates over the prediction horizon, i.e., β_n^{max} and γ_n^{max} . We then apply the adaptive thresholding over the maximum parameter set of all regions, i.e., $\{\beta_n^{\text{max}}\}_N$ and $\{\gamma_n^{\text{max}}\}_N$ with quantile κ_{β} and κ_{γ} , to obtain adaptive thresholds β_{thr} and γ_{thr} . A region with both small β_n^{max} and γ_n^{max} would be detected:

$$f_n^{\text{small}} = \mathbb{I}(\beta_n^{\text{max}} \leq \beta_{\text{thr}} \wedge \gamma_n^{\text{max}} \leq \gamma_{\text{thr}}) \quad (12)$$

Low Infection Detection. Low infection detection aims to detect whether the infection population of a region is sufficiently small. We first apply the adaptive thresholding on $\mathbf{I}^{t-(T_{\text{in}}-1):t}$ with quantile κ_I to obtain a global near-zero threshold I_{abs} . Then, for each region n , the proportion of near-zero infection days can be defined as $\rho_n = \frac{1}{T_{\text{in}}} \sum_{\tau=t-(T_{\text{in}}-1)}^t \mathbb{I}(I_n^{\tau} \leq I_{\text{abs}})$. We then apply the adaptive thresholding over $\{\rho_n\}_N$ with quantile κ_{ρ} to obtain $\hat{\kappa}_{\text{ZR}}$. To maintain suppression sensitivity, we cap the threshold by $\kappa_{\rho}^{\text{max}}$, i.e., $\hat{\kappa}_{\text{ZR}} \leftarrow \min(\hat{\kappa}_{\text{ZR}}, \kappa_{\rho}^{\text{max}})$. A region with proportion of near-zero infection days larger than $\hat{\kappa}_{\text{ZR}}$ would be detected:

$$f_n^{\text{quiet}} = \mathbb{I}(\rho_n \geq \hat{\kappa}_{\text{ZR}}), \quad (13)$$

Suppressed Metapopulation SIR. The final suppression filter is defined as the union of two detection results, i.e., $f_n = f_n^{\text{quiet}} \vee f_n^{\text{small}}$. We apply the filter to adaptively suppress the disease transmission process by modifying the infection parameter β_n in the MetaSIR model [Wang *et al.*, 2018], which is achieved as follows:

$$\hat{\beta}_n = \psi^{f_n} \beta_n \quad (14)$$

where $\psi \in (0, 1)$ is a small constant for downscaling. Based on the revised infection update equation, we can obtain the daily confirmed cases prediction according to MetaSIR [Wang *et al.*, 2018]. During the training time, the model is optimized via Mean Absolute Error (MAE) loss.

4 Experiments

We evaluate the performance of the proposed method on two real-world epidemic datasets.

4.1 Datasets

To validate the applicability of the proposed model, we conducted evaluation on two types of epidemic datasets with unique characteristics, which are summarized as follows:

- **COVID-19 Dataset.** This dataset contains daily confirmed COVID-19 cases in 47 prefectures in Japan covering the period from April 1, 2020, to September 21, 2021 (539 days) from the NHK COVID-19². Other related observations are

²<https://www3.nhk.or.jp/news/special/coronavirus/data/>

Table 1: Results on the **COVID-19** dataset across different horizons (STOEP’s improvements are statistically significant, with p -value $< 2 \times 10^{-4}$ across all baselines).

Model	3 d Ahead				7 d Ahead				14 d Ahead				Overall			
	RMSE	MAE	SMAPE	RAE	RMSE	MAE	SMAPE	RAE	RMSE	MAE	SMAPE	RAE	RMSE	MAE	SMAPE	RAE
SIR [1927]	441.0	156.5	84.1	0.49	522.3	195.2	113.3	0.58	932.1	322.9	133.2	0.97	616.8	214.6	102.7	0.65
MetaSIR [KDD18]	346.8	128.4	72.7	0.39	412.4	167.8	94.8	0.51	795.4	283.2	129.7	0.84	517.4	184.3	110.4	0.54
STGCN [IJCAI18]	372.9	117.0	44.9	0.36	378.5	127.0	52.1	0.38	427.9	158.5	74.2	0.48	388.4	131.6	55.3	0.40
MTGNN [KDD20]	307.2	105.8	41.1	0.32	382.4	137.5	50.1	0.41	443.5	168.3	80.2	0.52	363.2	135.0	50.7	0.49
CovidGNN [2020]	288.4	96.8	45.1	0.29	339.1	127.9	63.4	0.38	443.3	185.0	114.4	0.55	358.2	133.4	68.4	0.40
DCRNN [ICLR18]	312.7	92.8	37.9	0.28	336.3	111.8	48.4	0.34	386.6	149.9	72.6	0.45	344.3	116.0	50.8	0.35
PopNet [WWW22]	330.4	128.1	57.6	0.39	331.9	130.6	56.8	0.39	398.3	157.7	67.2	0.48	341.3	133.0	58.5	0.40
TimeKAN [ICLR25]	327.4	124.8	55.8	0.38	330.8	129.4	58.5	0.39	329.8	130.0	61.7	0.39	329.1	127.8	57.6	0.39
COVID-Forecaster [ICDE23]	318.6	106.7	50.0	0.32	322.1	118.7	58.8	0.35	331.9	140.9	80.1	0.42	324.0	121.4	62.2	0.37
GraphWaveNet [IJCAI19]	234.2	76.5	47.3	0.22	315.1	105.5	57.7	0.32	308.4	148.1	76.6	0.44	315.1	105.5	57.7	0.32
LightGTS [ICML25]	254.7	88.4	39.1	0.27	284.0	104.9	48.0	0.31	379.8	149.3	72.1	0.45	306.2	111.0	50.4	0.33
ColaGNN [CIKM20]	242.0	76.3	40.2	0.23	337.4	119.9	43.9	0.37	376.1	147.5	69.9	0.43	294.2	106.4	50.2	0.33
AMD [AAAI25]	287.5	113.0	65.0	0.34	291.0	115.5	65.3	0.34	291.7	115.3	63.7	0.34	289.8	114.7	65.2	0.34
STDDE [WWW24]	277.5	105.2	51.9	0.32	277.0	107.2	51.6	0.32	276.9	108.2	53.1	0.33	277.1	107.0	52.1	0.32
PDFormer [AAAI23]	273.1	97.7	<u>36.6</u>	0.29	269.2	97.8	44.2	0.29	275.5	103.6	62.5	0.31	272.2	99.5	<u>46.3</u>	0.30
DUET [KDD25]	275.6	100.8	43.2	0.30	271.3	101.2	<u>44.0</u>	0.30	267.6	<u>101.9</u>	63.0	<u>0.30</u>	271.6	101.3	46.5	0.30
AGCRN [NeurIPS20]	209.1	76.1	49.9	0.23	234.0	94.1	55.7	0.28	336.9	143.2	81.5	0.43	253.5	103.0	60.0	0.31
STAN [JAMIA21]	330.6	127.8	57.0	0.39	365.4	143.9	62.8	0.43	398.9	158.6	70.1	0.48	348.4	136.8	60.3	0.41
CausalGNN [AAAI22]	308.8	104.4	39.6	0.32	313.6	116.8	46.4	0.35	331.9	149.2	67.1	0.45	317.1	121.4	49.9	0.37
MPSTAN [Entropy24]	302.1	127.0	51.4	0.38	316.8	137.5	54.3	0.41	331.9	147.4	60.6	0.44	316.1	136.7	54.9	0.41
MepoGNN [ECML-PKDD22]	<u>139.2</u>	<u>54.9</u>	37.6	<u>0.17</u>	<u>177.5</u>	<u>72.8</u>	45.5	<u>0.22</u>	<u>250.6</u>	103.8	<u>61.1</u>	0.31	<u>188.5</u>	<u>75.5</u>	47.1	<u>0.23</u>
STOEP (Ours)	125.3	49.8	35.9	0.15	149.3	63.1	43.1	0.19	230.1	97.9	61.6	0.29	169.1	68.8	45.4	0.21

from the Ministry of Health, Labour and Welfare, etc. The mobility data are from Facebook Movement Range Maps³. The entire dataset is publicly available⁴.

- **Flu Dataset.** This dataset contains daily confirmed flu cases in 11 cities of a provincial CDC in China, for 2023-2024 (731 days). We can derive the daily susceptible/infected/recovered population from it in a similar way as COVID-19 dataset did. The mobility data are from Baidu Migration Map⁵.

The detailed demographic and mobility characteristics of both datasets can be found in Appendix B.

For each dataset, we partition it into non-overlapped train, validation and test set chronologically by a ratio of 6:1:1.

4.2 Experimental Settings

Baselines. We compare our proposed method with three categories of baselines:

- **Mechanistic Models:** SIR [Kermack and McKendrick, 1927] and MetaSIR [Wang *et al.*, 2018].
- **Deep Learning Models:** (1) *Time-series Models:* AMD [Hu *et al.*, 2025], TimeKAN [Huang *et al.*, 2025], DUET [Qiu *et al.*, 2025], LightGTS [Wang *et al.*, 2025]; (2) *Spatio-temporal Graph Models:* DCRNN [Li *et al.*, 2018], STGCN [Yu *et al.*, 2018], GraphWaveNet [Wu *et al.*, 2019], ColaGNN [Deng *et al.*, 2020], MTGNN [Wu *et al.*, 2020], AGCRN [Bai *et al.*, 2020], CovidGNN [Kapoor *et al.*, 2020], PopNet [Gao *et al.*, 2022], STDDE [Long *et al.*, 2024].

³<https://data.humdata.org/dataset/movement-range-maps>

⁴<https://github.com/deepkashiwa20/MepoGNN>

⁵<https://qianxi.baidu.com/>

- **Hybrid Models:** STAN [Gao *et al.*, 2021], MPSTAN [Mao *et al.*, 2024], CausalGNN [Wang *et al.*, 2022], MepoGNN [Cao *et al.*, 2022].

Detailed descriptions can be found in Appendix C.

Evaluation Methods. Following previous work [Tang *et al.*, 2023; Cao *et al.*, 2022], we evaluate the 3d, 7d, 14d, and overall prediction performance of our model by four metrics, i.e., Rooted Mean Squared Error (RMSE), Mean Absolute Error (MAE), Symmetric Mean Absolute Percentage Error (SMAPE), and Relative Absolute Error (RAE).

Implementation & Training Settings. We implement STOEP and baselines using PyTorch on an NVIDIA RTX 5060 GPU. The model is optimized via Adam with a curriculum learning strategy. Detailed configurations and training settings can be found in Appendix D.

4.3 Overall Evaluation

Table 1 summarizes the results of different methods on the COVID-19 dataset against all baselines. STOEP consistently achieves the best performance across almost all horizons and metrics. On the overall results, it obtains 10.3% lower RMSE, 8.9% lower MAE, and 8.7% lower RAE than MepoGNN, highlighting a substantial improvement in both accuracy and robustness. The advantage is particularly evident on the 7-day horizon, where STOEP achieves 15.9% lower RMSE and 13.3% lower MAE, demonstrating its superiority in mid-term forecasting.

Table 2 summarizes results on the Flu dataset. STOEP again delivers the best performance across all horizons and metrics. Compared with MepoGNN on the overall results, it achieves 11.8% lower RMSE, 9.0% lower MAE and 7.5% lower RAE. On the 7-day horizon, STOEP reduces RMSE

Table 2: Results on the **Flu** dataset across different horizons (STOEP’s improvements are statistically significant, with p -value $< 2 \times 10^{-4}$ across all baselines).

Model	3 d Ahead				7 d Ahead				14 d Ahead				Overall			
	RMSE	MAE	SMAPE	RAE												
SIR [1927]	148.5	92.1	193.8	1.04	150.2	93.0	195.2	1.04	147.3	91.0	196.8	1.05	149.4	92.5	195.1	1.04
MetaSIR [KDD18]	88.4	56.5	64.2	0.64	124.6	80.3	80.3	0.90	199.4	125.9	100.4	1.46	137.3	83.9	79.9	0.95
STGCN [IJCAI18]	62.2	29.7	32.7	0.34	93.9	45.5	42.0	0.51	113.7	52.4	47.6	0.61	92.3	42.5	40.7	0.48
MTGNN [KDD20]	135.3	81.1	64.9	0.92	144.2	88.6	73.4	0.99	150.5	93.6	78.7	1.08	143.4	87.6	71.9	0.88
CovidGNN [2020]	152.3	136.5	113.4	1.54	157.5	142.2	115.5	1.60	167.0	152.3	119.6	1.76	157.3	141.9	115.7	1.60
DCRNN [ICLR18]	57.2	28.0	32.6	0.32	81.5	40.6	41.0	0.46	95.8	47.0	46.7	0.54	80.7	38.9	40.1	0.44
PopNet [WWW22]	122.9	78.6	95.7	0.89	124.0	78.8	95.3	0.88	121.1	76.6	95.1	0.89	123.3	78.4	95.4	0.89
ColaGNN [CIKM20]	125.2	110.5	109.4	1.25	127.2	112.9	110.2	1.27	129.4	116.7	112.1	1.35	126.7	112.1	110.0	1.27
TimeKAN [ICLR25]	117.9	83.8	98.9	0.95	122.6	77.3	118.6	0.87	121.3	84.4	99.3	0.98	126.9	86.6	113.2	0.98
COVID-Forecaster [ICDE23]	119.5	69.6	87.9	0.79	122.7	72.0	89.3	0.81	121.7	70.7	89.8	0.82	122.5	71.5	89.2	0.81
GraphWaveNet [IJCAI19]	56.8	27.7	32.4	0.31	80.3	39.5	<u>40.2</u>	0.44	94.1	45.9	<u>46.0</u>	0.53	79.1	37.7	<u>39.3</u>	0.43
LightGTS [ICML25]	94.5	53.7	71.9	0.61	95.8	54.5	72.6	0.61	93.4	53.0	72.2	0.61	95.1	54.1	72.4	0.61
AMD [AAAI25]	113.6	68.2	90.2	0.77	145.3	88.2	150.1	0.99	129.8	74.9	106.3	0.87	133.0	79.3	118.4	0.90
STDDE [WWW24]	93.8	54.8	67.3	0.62	96.8	57.4	70.5	0.64	96.0	57.3	72.2	0.66	96.2	56.9	69.8	0.64
PDFormer [AAAI23]	137.6	78.5	94.3	0.89	137.9	78.6	94.8	0.88	135.5	76.8	95.8	0.89	136.2	77.6	93.6	0.88
DUET [KDD25]	111.8	70.8	80.4	0.80	116.6	73.9	82.6	0.83	147.6	91.1	183.8	1.05	116.7	72.6	88.7	0.82
AGCRN [NeurIPS20]	139.9	81.1	101.4	0.92	141.0	81.5	102.2	0.91	137.7	79.1	102.2	0.92	140.2	81.1	102.0	0.92
STAN [JAMIA21]	149.9	93.3	184.0	1.05	151.0	93.7	183.6	1.05	147.5	91.0	183.0	1.05	150.2	93.2	183.7	1.05
CausalGNN [AAAI22]	121.5	78.3	96.8	0.88	124.0	78.7	96.2	0.88	121.6	76.6	95.5	0.89	123.1	78.3	96.1	0.88
MPSTAN [Entropy24]	74.3	43.1	61.0	0.49	83.5	47.3	63.8	0.53	88.7	49.3	66.3	0.57	82.6	46.7	63.5	0.53
MepoGNN [ECML-PKDD22]	<u>54.1</u>	<u>26.4</u>	<u>32.0</u>	<u>0.30</u>	<u>72.9</u>	<u>37.2</u>	40.9	<u>0.42</u>	<u>84.0</u>	<u>43.2</u>	46.7	<u>0.50</u>	<u>72.0</u>	<u>35.6</u>	39.8	<u>0.40</u>
STOEP (Ours)	51.9	24.8	31.6	0.28	65.2	34.4	39.8	0.39	70.5	37.8	45.3	0.44	63.5	32.4	38.8	0.37

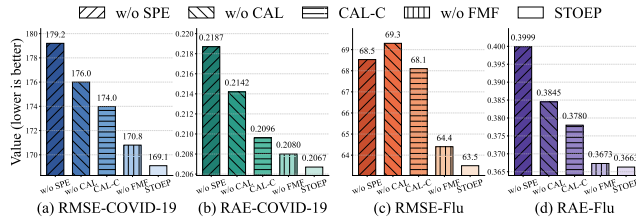


Figure 3: Ablation on the COVID-19 and Flu dataset.

and MAE by 10.6% and 7.5%, respectively, underscoring stable mid-term benefits in a real operational setting.

The significance test confirms that STOEP’s improvements are statistically significant, with a permutation p -value $< 2 \times 10^{-4}$ across all baselines.

4.4 Ablation Study

We conduct ablation experiments on both datasets to quantify the contribution of each component in STOEP by comparing the following variants: *w/o SPE* keeps the architecture of SPE module but routes its inputs through a 1×1 convolution whose output is directly fed into GraphWaveNet for parameter estimation. *w/o CAL* removes the case-based adjacency intensity. *CAL-C* uses k -shape clustering [Paparrizos and Gravano, 2015] within the CAL module to obtain temporal patterns instead of self-learned patterns. *w/o FMF* replaces the FMF module with a classic MetaSIR for forecasting.

As shown in Figure 3, Space-informed Parameter Estimation provides the largest benefit, and STOEP lowers RMSE by 5.6% and RAE by 5.5% on the COVID-19 dataset, while on the Flu dataset, it lowers RMSE by 7.3% and RAE by

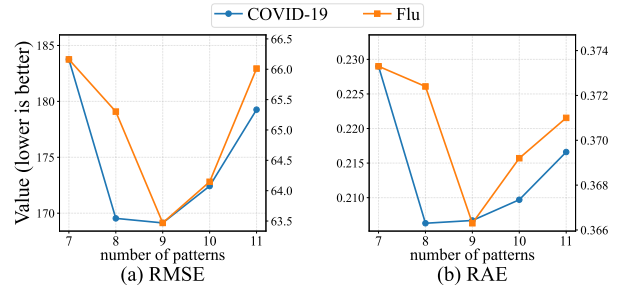


Figure 4: Different number of patterns P .

8.4%, compared to *w/o SPE*. The CAL module significantly reduced the RMSE by 8.3% on the Flu dataset. While the CAL-C variant performed better than the *w/o CAL* variant, it was inferior to STOEP on both datasets. This suggests that the self-learned patterns are more effective than using clustering. After the disease transmission suppression in FMF is removed, i.e., *w/o SMF*, RMSE is increased by 1.4% on the Flu dataset, which also demonstrates its effectiveness in suppressing unstable parameter estimation.

4.5 Hyperparameter Sensitivity

We further analyzed the sensitivity of the proposed model with respect to the number of learned patterns in the CAL module. Figure 4 reports the results for RMSE and RAE as the number of patterns varies from 7 to 11 on both the COVID-19 dataset and the Flu dataset. Overall, the performance is relatively stable across different settings, but performance is generally optimal at 9 patterns. These results suggest that a moderate number of patterns is sufficient to capture

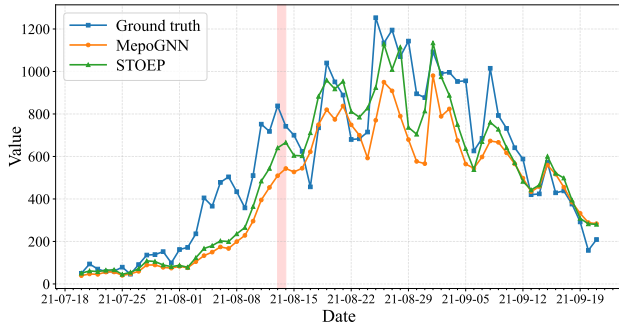


Figure 5: Predicted daily confirmed cases of COVID-19 with horizon = 7.

the temporal dynamics without introducing redundancy.

4.6 Case Study

To further demonstrate the effectiveness of STOEP, we have conducted case studies on STOEP and the most competitive forecasting model, i.e., MepoGNN. We visualize the prediction results (7d ahead) of STOEP and MepoGNN from July 18, 2021, to September 19, 2021, on COVID-19 dataset in Figure 5, where the blue line represents the ground-truth. It can be observed that our model is closer to the ground-truth than MepoGNN and more capable of capturing the occurrence of peaks. For instance, STOEP successfully predicted a peak around August 13-14, a period when Delta variant was prevalent in Japan and the epidemic was expanding rapidly⁶. This indicates that our model can reflect real-world scenarios more accurately than MepoGNN.

The case study on the Flu dataset is also conducted which demonstrates STOEP’s ability to capture seasonal peaks and delayed propagation. Details refer to Appendix E.

4.7 System Deployment

A system based on STOEP has already been deployed in one provincial CDC in China, providing daily influenza forecasts for 11 cities. As shown in Figure 6, the system utilizes our model to visualize real-time trends and risk levels. Public health practitioners can use the system to trigger the early warning of infectious diseases and precisely allocate medical resources among regions in advance.

5 Related Work

Epidemic forecasting can be mainly categorized into three types: mechanistic models, data-driven models, and hybrid models. (1) **Mechanistic models** model the infecting dynamics across different groups of populations, i.e., compartments, using differential equations, e.g., SIR model [Kermack and McKendrick, 1927; Rizoio *et al.*, 2018], SEIR model [Wang *et al.*, 2024]. Considering the spatial heterogeneity, MetaSIR [Wang *et al.*, 2018] is further proposed to

⁶<https://www.reuters.com/world/asia-pacific/japanese-regions-see-record-covid-19-infections-delta-variant-spreads-media-2021-08-18/>

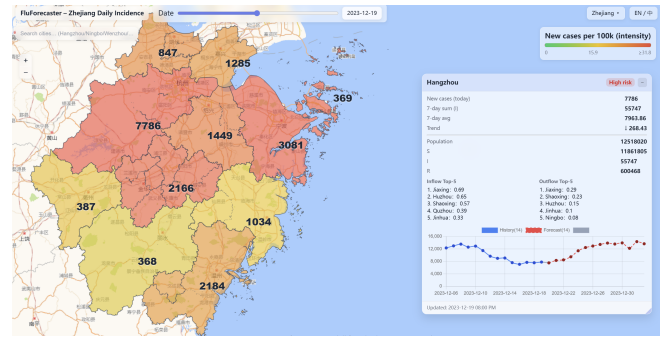


Figure 6: Screenshot of the deployed system based on STOEP in a provincial CDC in China.

jointly forecast for several regions. However, they usually rely on experts’ knowledge and strong assumptions on disease transmission, which limit their prediction capability. (2) **Data-driven models** can flexibly learn to forecast based on past observations. Auto-Regressive model [Perrotta *et al.*, 2017], ARIMA [Kufel, 2020] are initially adopted. In the era of deep learning, Bi-LSTM [Arora *et al.*, 2020] are commonly used. For spatio-temporal forecasting, the spatial dependency among different regions can be constructed based on region adjacency [Deng *et al.*, 2020; Kapoor *et al.*, 2020], mobility intensity [Gao *et al.*, 2022], or self-attention [Shen *et al.*, 2023]. Though data-driven models show superior performance, they learn parameters purely based on data, which makes them have limited generalization capability. (3) **Hybrid models** combine the mechanistic models and powerful modeling ability of deep learning. STAN [Gao *et al.*, 2021] and PISID [Fujita and Akutsu, 2025] regulate the network training loss with SIR constraints, while MPSTAN [Mao *et al.*, 2024] adds the MetaSIR module into the recurrent cell. MepoGNN [Cao *et al.*, 2022], CausalGNN [Wang *et al.*, 2022] and EISTGNN [Han *et al.*, 2025] estimate epidemic parameters of mechanistic models by neural networks. However, EISTGNN is not directly comparable to us because it focuses on latent graph learning without external topology, differing from our setting which explicitly incorporates mobility data. Our proposed method also belong to this category. However, different from previous work, we enhance the models with spatio-temporal priors via CAL and SPE, and expert priors via FMF.

6 Conclusion

In this paper, we propose STOEP, a spatio-temporal prior-aware epidemic predictor, which enhances the hybrid model by prior knowledge. Spatio-temporal priors are injected into the adjacency learning and amplify the input signals, while expert priors guide the design of parameter adaptive thresholding. Experiments on COVID-19 and influenza datasets show that STOEP consistently outperforms the best baseline by 11.1% on average in RMSE. A system based on STOEP is also deployed in a provincial CDC in China for forecasting to facilitate downstream applications. Further investigation into the cross-regional and cross-disease transferability of the proposed model is warranted.

References

- [Arora *et al.*, 2020] Parul Arora, Himanshu Kumar, and Bijaya Ketan Panigrahi. Prediction and analysis of covid-19 positive cases using deep learning models: A descriptive case study of india. *Chaos, solitons & fractals*, 139:110017, 2020.
- [Bai *et al.*, 2020] Lei Bai, Lina Yao, Can Li, Xianzhi Wang, and Can Wang. Adaptive graph convolutional recurrent network for traffic forecasting. *Advances in neural information processing systems*, 33:17804–17815, 2020.
- [Cao *et al.*, 2022] Qi Cao, Renhe Jiang, Chuang Yang, Zipei Fan, Xuan Song, and Ryosuke Shibasaki. Mepognn: Metapopulation epidemic forecasting with graph neural networks. In *Joint European Conference on Machine Learning and Knowledge Discovery in Databases*, pages 453–468, 2022.
- [Deng *et al.*, 2020] Songgaojun Deng, Shusen Wang, Huzefa Rangwala, Lijing Wang, and Yue Ning. Cola-gnn: Cross-location attention based graph neural networks for long-term ili prediction. In *Proceedings of the 29th ACM international conference on information & knowledge management*, pages 245–254, 2020.
- [Fujita and Akutsu, 2025] Satoki Fujita and Tatsuya Akutsu. Enhancing epidemic forecasting with a physics-informed spatial identity neural network. *PLoS One*, 20(9):e0331611, 2025.
- [Gao *et al.*, 2021] Junyi Gao, Rakshith Sharma, Cheng Qian, Lucas M Glass, Jeffrey Spaeder, Justin Romberg, Jimeng Sun, and Cao Xiao. Stan: spatio-temporal attention network for pandemic prediction using real-world evidence. *Journal of the American Medical Informatics Association*, 28(4):733–743, 2021.
- [Gao *et al.*, 2022] Junyi Gao, Cao Xiao, Lucas M Glass, and Jimeng Sun. Popnet: Real-time population-level disease prediction with data latency. In *Proceedings of the ACM Web Conference 2022*, pages 2552–2562, 2022.
- [Han *et al.*, 2025] Shuai Han, Lukas Stelz, Thomas R Sokolowski, Kai Zhou, and Horst Stöcker. Epidemiology-informed spatiotemporal graph neural network for heterogeneity-driven interpretable epidemic forecasting. *Engineering Applications of Artificial Intelligence*, 162:112764, 2025.
- [Hu *et al.*, 2025] Yifan Hu, Peiyuan Liu, Peng Zhu, Dawei Cheng, and Tao Dai. Adaptive multi-scale decomposition framework for time series forecasting. In *Proceedings of the AAAI Conference on Artificial Intelligence*, 2025.
- [Huang *et al.*, 2025] Songtao Huang, Zhen Zhao, Can Li, and LEI BAI. TimeKAN: KAN-based frequency decomposition learning architecture for long-term time series forecasting. In *The Thirteenth International Conference on Learning Representations*, 2025.
- [Kapoor *et al.*, 2020] Amol Kapoor, Xue Ben, Luyang Liu, Bryan Perozzi, Matt Barnes, Martin Blais, and Shawn O’Banion. Examining covid-19 forecasting using spatio-temporal graph neural networks. 2020.
- [Kermack and McKendrick, 1927] William Ogilvy Kermack and Anderson G McKendrick. A contribution to the mathematical theory of epidemics. *Proceedings of the royal society of london. Series A, Containing papers of a mathematical and physical character*, 115(772):700–721, 1927.
- [Kingma, 2014] DP Kingma. Adam: a method for stochastic optimization. In *Int Conf Learn Represent*, 2014.
- [Kufel, 2020] Tadeusz Kufel. Arima-based forecasting of the dynamics of confirmed covid-19 cases for selected european countries. *Equilibrium. Quarterly Journal of Economics and Economic Policy*, 15(2):181–204, 2020.
- [Li *et al.*, 2018] Yaguang Li, Rose Yu, Cyrus Shahabi, and Yan Liu. Diffusion convolutional recurrent neural network: Data-driven traffic forecasting. In *International Conference on Learning Representations*, 2018.
- [Long *et al.*, 2024] Qingqing Long, Zheng Fang, Chen Fang, Chong Chen, Pengfei Wang, and Yuanchun Zhou. Unveiling delay effects in traffic forecasting: a perspective from spatial-temporal delay differential equations. In *Proceedings of the ACM Web Conference 2024*, pages 1035–1044, 2024.
- [Mao *et al.*, 2024] Junkai Mao, Yuexing Han, and Bing Wang. Mpstan: Metapopulation-based spatio-temporal attention network for epidemic forecasting. *Entropy*, 26(4):278, 2024.
- [Paparrizos and Gravano, 2015] John Paparrizos and Luis Gravano. k-shape: Efficient and accurate clustering of time series. In *Proceedings of the 2015 ACM SIGMOD international conference on management of data*, pages 1855–1870, 2015.
- [Perrotta *et al.*, 2017] Daniela Perrotta, Michele Tizzoni, and Daniela Paolotti. Using participatory web-based surveillance data to improve seasonal influenza forecasting in italy. In *Proceedings of the 26th International Conference on World Wide Web*, pages 303–310, 2017.
- [Qian *et al.*, 2021] Zhaozhi Qian, Ahmed M Alaa, and Michaela van der Schaar. Cpas: the uk’s national machine learning-based hospital capacity planning system for covid-19. *Machine Learning*, 110(1):15–35, 2021.
- [Qiu *et al.*, 2025] Xiangfei Qiu, Xingjian Wu, Yan Lin, Chenjuan Guo, Jilin Hu, and Bin Yang. Duet: Dual clustering enhanced multivariate time series forecasting. In *SIGKDD*, pages 1185–1196, 2025.
- [Rizoiu *et al.*, 2018] Marian-Andrei Rizoiu, Swapnil Mishra, Quyu Kong, Mark Carman, and Lexing Xie. Sirhawkes: Linking epidemic models and hawkes processes to model diffusions in finite populations. In *Proceedings of the 2018 world wide web conference*, pages 419–428, 2018.
- [Shen *et al.*, 2023] Tong Shen, Yang Li, and José MF Moura. Forecasting covid-19 dynamics: Clustering, generalized spatiotemporal attention, and impacts of mobility and geographic proximity. In *2023 IEEE 39th International Conference on Data Engineering (ICDE)*, pages 2892–2904. IEEE, 2023.

- [Tang *et al.*, 2023] Yinzhou Tang, Huandong Wang, and Yong Li. Enhancing spatial spread prediction of infectious diseases through integrating multi-scale human mobility dynamics. In *Proceedings of the 31st ACM International Conference on Advances in Geographic Information Systems*, pages 1–12, 2023.
- [Wang *et al.*, 2018] Jingyuan Wang, Xiaojian Wang, and Junjie Wu. Inferring metapopulation propagation network for intra-city epidemic control and prevention. In *Proceedings of the 24th ACM SIGKDD International Conference on Knowledge Discovery & Data Mining*, pages 830–838. ACM, 2018.
- [Wang *et al.*, 2022] Lijing Wang, Aniruddha Adiga, Jiangzhuo Chen, Adam Sadilek, Srinivasan Venkatramanan, and Madhav Marathe. Causalgnn: Causal-based graph neural networks for spatio-temporal epidemic forecasting. In *Proceedings of the AAAI conference on artificial intelligence*, volume 36, pages 12191–12199, 2022.
- [Wang *et al.*, 2024] Yiheng Wang, Guanjie Zheng, Hexi Jin, Yi Sun, Kan Wu, and Jie Fang. Precise control balances epidemic mitigation and economic growth. *npj Urban Sustainability*, 4(1):28, 2024.
- [Wang *et al.*, 2025] Yihang Wang, Yuying Qiu, Peng Chen, Yang Shu, Zhongwen Rao, Lujia Pan, Bin Yang, and Chenjuan Guo. Lightgts: A lightweight general time series forecasting model. In *Forty-second International Conference on Machine Learning*, 2025.
- [Wu *et al.*, 2019] Zonghan Wu, Shirui Pan, Guodong Long, Jing Jiang, and Chengqi Zhang. Graph wavenet for deep spatial-temporal graph modeling. In *Proceedings of the 28th International Joint Conference on Artificial Intelligence*, pages 1907–1913, 2019.
- [Wu *et al.*, 2020] Zonghan Wu, Shirui Pan, Guodong Long, Jing Jiang, Xiaojun Chang, and Chengqi Zhang. Connecting the dots: Multivariate time series forecasting with graph neural networks. In *Proceedings of the 26th ACM SIGKDD international conference on knowledge discovery & data mining*, pages 753–763, 2020.
- [Yu *et al.*, 2018] Bing Yu, Haoteng Yin, and Zhanxing Zhu. Spatio-temporal graph convolutional networks: A deep learning framework for traffic forecasting. In *Proceedings of the Twenty-Seventh International Joint Conference on Artificial Intelligence*, pages 3634–3640. International Joint Conferences on Artificial Intelligence Organization, 2018.

A Complexity and Scalability Analysis

We analyze the computational complexity of STOEP to assess its efficiency and scalability. Let N denote the number of regions, T_{in} the input sequence length, T_{out} the forecasting horizon, and C the feature dimension. Batch size and other constant factors are omitted for clarity.

Time Complexity. The dominant computational cost of STOEP arises from dense region-to-region interactions. The dynamic adjacency learning and spatial modeling operations involve $N \times N$ matrix computations, while spatial attention and graph convolution are applied across the temporal dimension. As a result, the overall time complexity of STOEP is

$$\mathcal{O}(N^2(T_{in}C + T_{out})) . \quad (15)$$

Space Complexity. STOEP requires memory to store dense adjacency matrices, mobility-related origin–destination tensors, and intermediate node representations. Specifically, the space complexity is dominated by the storage of $N \times N$ matrices across both input and prediction horizons, leading to

$$\mathcal{O}((T_{in} + T_{out})N^2 + T_{in}NC) \quad (16)$$

memory usage.

Scalability. Although STOEP exhibits a quadratic dependency on the number of regions, this design is well suited for epidemic forecasting tasks at the city or prefecture level, where the number of regions typically ranges from tens to a few hundreds, making the model computationally practical in real-world settings.

B Dataset Characteristics and Generalizability Analysis

To thoroughly assess the robustness of STOEP against demographic bias and diverse epidemic dynamics, we analyze the statistical properties of the two datasets used in our evaluation.

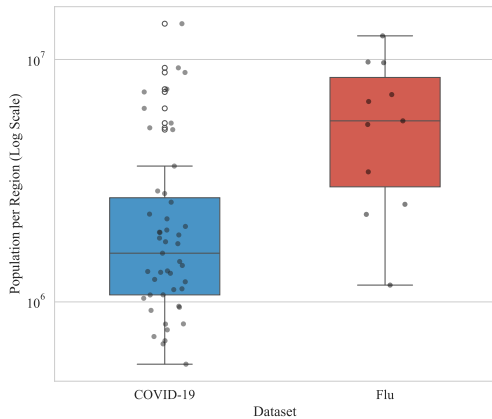


Figure 7: Comparison of regional population distributions (Log Scale). The COVID-19 dataset covers a national scale with high variance, while the Flu dataset represents a provincial scale.

Demographic Scale. As illustrated in Figure 7, the two datasets represent distinct demographic scales. The Japan dataset covers a national scale ($N = 47$ prefectures) with a high variance in population sizes, ranging from major metropolitan areas to rural prefectures. In contrast, the Zhejiang dataset focuses on a provincial scale ($N = 11$ cities) characterized by relatively denser and more uniform urban populations. This difference allows us to validate STOEP’s performance across varying administrative granularities.

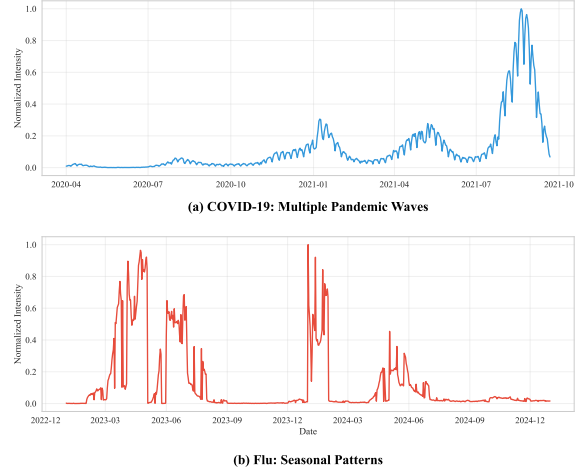


Figure 8: Normalized daily confirmed cases. (Top) COVID-19 in Japan exhibits multiple pandemic waves driven by variants. (Bottom) Flu in China shows characteristic seasonal peaks.

Epidemic Dynamics. Figure 8 visualizes the normalized daily confirmed cases to highlight the temporal patterns of the diseases while preserving data privacy. The COVID-19 dataset exhibits complex, irregular pandemic waves driven by the emergence of new variants. Conversely, the Flu dataset demonstrates distinct seasonal peaks typical of influenza. STOEP’s superior performance on both datasets confirms its capability to generalize across biologically distinct pathogens.

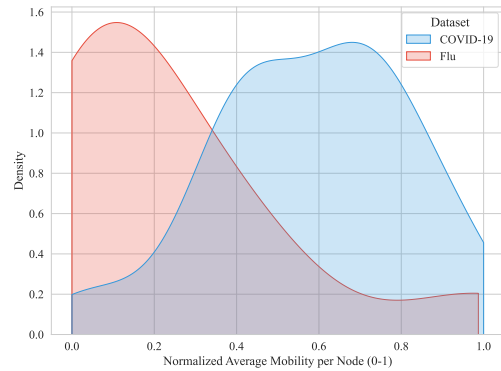


Figure 9: Distribution of normalized average mobility intensity per node. Despite different sources (Facebook vs. Baidu), both datasets provide rich mobility heterogeneity.

Mobility Distribution. We also analyze the mobility data characteristics in Figure 9. The COVID-19 dataset utilizes Facebook Movement Range Maps, while the Flu dataset uses Baidu Migration Map data. Despite originating from different providers with different raw scales, the normalized distribution shows that both datasets provide rich heterogeneity in mobility intensity. STOEP effectively leverages these diverse mobility signals to enhance adjacency learning.

In summary, by demonstrating consistent improvements across diverse settings, encompassing national and provincial demographics, pandemic and seasonal disease dynamics, and distinct mobility data sources, STOEP evidences strong generalizability and robustness against potential demographic biases.

C Detailed Baseline Descriptions

We compare our proposed method with three types of baselines as mentioned in Section 5: 1) Mechanistic Models, 2) Deep Learning Models, and 3) Hybrid Models. We detail them as follows:

1. **Mechanistic Models.** We select two representative methods, i.e., SIR [Kermack and McKendrick, 1927] and MetaSIR [Wang *et al.*, 2018].
2. **Deep Learning Models.** We compare the proposed method with epidemic-specific deep learning models as well as general time-series or spatio-temporal models, which are further categorized as follows:
 - Time-series Models, which include AMD [Hu *et al.*, 2025], TimeKAN [Huang *et al.*, 2025], DUET [Qiu *et al.*, 2025], LightGTS [Wang *et al.*, 2025]. To adapt to the spatio-temporal epidemic forecasting problem, we transform the historical observations into a matrix by flattening the region and factor dimensions. Besides, to further integrate the mobility data, we flatten, embed and concatenate it with other observations. The model outputs are transformed back to the region dimension to obtain the final predictions.
 - Spatio-temporal Graph Models, which construct a spatial graph to model spatial dependency, including DCRNN [Li *et al.*, 2018], STGCN [Yu *et al.*, 2018], GraphWaveNet [Wu *et al.*, 2019], ColaGNN [Deng *et al.*, 2020], MTGNN [Wu *et al.*, 2020], AGCRN [Bai *et al.*, 2020], CovidGNN [Kapoor *et al.*, 2020], PopNet [Gao *et al.*, 2022] and STDDE [Long *et al.*, 2024]. Among them, only CovidGNN [Kapoor *et al.*, 2020] leverages the mobility data to set the edge weights. For DCRNN [Li *et al.*, 2018], STGCN [Yu *et al.*, 2018], PopNet [Gao *et al.*, 2022], and STDDE [Long *et al.*, 2024], we follow a common practice by constructing a static spatial graph where the edge weights are derived from average inter-region mobility flows. For other graph models that learn dynamic adjacency matrices, the time-varying mobility graph is integrated through temporal weighted fusion with the learned dynamic graph.

3. **Hybrid Models.** We compare network-dominated forecasters, i.e., STAN [Gao *et al.*, 2021], MPSTAN [Mao *et al.*, 2024], as well as mechanism-dominated forecasters, i.e., CausalGNN [Wang *et al.*, 2022], MepoGNN [Cao *et al.*, 2022]. Among them, MepoGNN [Cao *et al.*, 2022] leverages the mobility data to derive the edge weights. For CausalGNN [Wang *et al.*, 2022], mobility information is incorporated by combining the attention-based dynamic graph and the time-varying mobility graph through weighted fusion. For other hybrid models, we follow a standard practice by constructing a static adjacency matrix where edge weights are derived from aggregated mobility data.

D Implementation and Training Details

The input time length T_{in} and output time length T_{out} are both set to 14 days, which means we use two-week historical observations to do the two-week prediction of daily confirmed cases. P is set to 9. H is set to 4. $\kappa_I, \kappa_\rho, \kappa_\beta$ and κ_γ are set to 0.1, 0.9, 0.2 and 0.2. η is 0.9. $\delta_{min}^I, \delta_{min}^\rho, \delta_{min}^\beta$ and δ_{min}^γ are set to 0.5, 0.7, $2e-3$ and $2e-3$. κ_p^{max} is set to 0.98. ψ is set to 0.5.

During the training, the batch size is set to 32. Following previous work [Cao *et al.*, 2022], we use the curriculum learning strategy [Wu *et al.*, 2020] to gradually increase the prediction horizon. Adam [Kingma, 2014] optimizer is used, where the learning rate is $1e-3$ and weight decay is $1e-8$. The training algorithm would either be early-stopped if the validation error did not decrease within 20 epochs or be stopped after 300 epochs.

We implement our model as well as baselines with Python and PyTorch, and train them on a server with an NVIDIA RTX 5060 GPU.

E Case Study on Flu Epidemic Parameters

We analyze the estimated epidemiological parameters to demonstrate the model’s interpretability. Figure 10 presents estimated β from July 2024 to December 2024 in the Flu dataset, where a larger β indicates that more susceptible individuals become infected. We can observe that STOEP exhibits three more distinct peaks than MepoGNN, indicating that STOEP is more capable of capturing the summer and winter epidemic season, and successfully captures a delayed

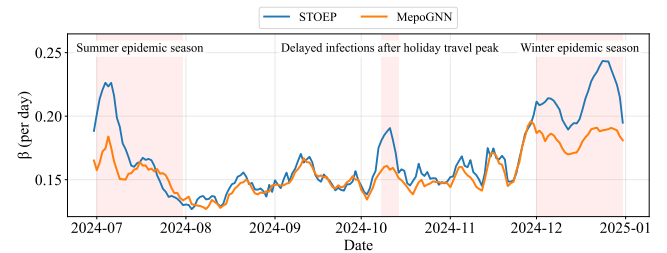


Figure 10: 7-day moving average of predicted β of Flu with horizon = 7.

epidemic peak induced by holiday travel in October, indicating that our model is better able to reflect infection peak periods.

F Metapopulation SIR

Metapopulation SIR model, i.e., MetaSIR [Wang *et al.*, 2018] extends classic SIR model [Kermack and McKendrick, 1927] by assuming the heterogeneity of regions and using human mobility to model the propagation among regions. For each region n , the mobility-induced transmission strength of region n at time $t + 1$, i.e., Π_n^{t+1} , is defined as:

$$\Pi_n^{t+1} = \sum_{m=1}^N \left(\frac{h_{nm}^{t+1}}{P_m} + \frac{h_{mn}^{t+1}}{P_n} \right) I_m^t, \quad (17)$$

where h_{nm}^{t+1} denotes the mobility flow from region n to m , P_m is the population size of region m , I_m^t is the infected population in region m . The epidemic dynamics for region n is as follows:

$$\begin{aligned} \frac{dS_n^{t+1}}{dt} &= -\beta_n^{t+1} \Pi_n^{t+1} \\ \frac{dI_n^{t+1}}{dt} &= \beta_n^{t+1} \Pi_n^{t+1} - \gamma_n^{t+1} I_n^t \\ \frac{dR_n^{t+1}}{dt} &= \gamma_n^{t+1} I_n^t \end{aligned} \quad (18)$$

where β_n^{t+1} and γ_n^{t+1} are the infection and recovery parameters of region n , and S_n^{t+1} , I_n^{t+1} , R_n^{t+1} denote the susceptible, infected, and recovered populations of region n at day $t + 1$. Based on the epidemic dynamics in Equation 18, S_n^{t+1} , I_n^{t+1} , R_n^{t+1} can be derived via differential equations, and the predicted daily confirmed cases of region n at day $t + 1$ can be calculated as:

$$\hat{x}_n^{t+1} = \beta_n^{t+1} \Pi_n^{t+1} \quad (19)$$

When this process is called recursively, we can obtain the multi-step daily confirmed case predictions $\hat{\mathbf{X}}^{t+1:t+T_{out}}$:

$$\hat{\mathbf{X}}^{t+1:t+T_{out}} = \begin{bmatrix} \hat{x}_1^{t+1} & \dots & \hat{x}_1^{t+T_{out}} \\ \vdots & \ddots & \vdots \\ \hat{x}_N^{t+1} & \dots & \hat{x}_N^{t+T_{out}} \end{bmatrix} \quad (20)$$

Classical SIR treats each region in isolation and relies on fixed-form infection and recovery dynamics, which limits its ability to capture mobility-driven transmission and to handle time-varying parameters robustly. The epidemic dynamics for region n follow:

$$\frac{dS_n^{t+1}}{dt} = -\beta_n^{t+1} I_n^t, \quad (21)$$

$$\frac{dI_n^{t+1}}{dt} = \beta_n^{t+1} I_n^t - \gamma_n^{t+1} I_n^t, \quad (22)$$

$$\frac{dR_n^{t+1}}{dt} = \gamma_n^{t+1} I_n^t, \quad (23)$$

where β_n^{t+1} and γ_n^{t+1} are the infection and recovery parameters of node n .